RESEARCH ARTICLE

PLANT GENETICS

Dominance hierarchy arising from the evolution of a complex small RNA regulatory network

Eléonore Durand,[1]* Raphaël Méheust,[1]* Marion Soucaze,[1] Pauline M. Goubet,[1]† Sophie Gallina,[1] Céline Poux,[1] Isabelle Fobis-Loisy,[2] Eline Guillon,[2] Thierry Gaude,[2] Alexis Sarazin,[3] Martin Figeac,[4] Elisa Prat,[5] William Marande,[5] Hélène Bergès,[5] Xavier Vekemans,[1] Sylvain Billiard,[1] Vincent Castric[1]‡

The prevention of fertilization through self-pollination (or pollination by a close relative) in the Brassicaceae plant family is determined by the genotype of the plant at the self-incompatibility locus (*S* locus). The many alleles at this locus exhibit a dominance hierarchy that determines which of the two allelic specificities of a heterozygous genotype is expressed at the phenotypic level. Here, we uncover the evolution of how at least 17 small RNA (sRNA)–producing loci and their multiple target sites collectively control the dominance hierarchy among alleles within the gene controlling the pollen *S*-locus phenotype in a self-incompatible *Arabidopsis* species. Selection has created a dynamic repertoire of sRNA-target interactions by jointly acting on sRNA genes and their target sites, which has resulted in a complex system of regulation among alleles.

Sporophytic self-incompatibility (SI) is a genetic system that evolved in hermaphroditic plants to enforce outcrossing (by preventing self-fertilization) and involves a polymorphism in which multiple alleles are maintained and display dominance-recessivity relations. In the genus *Arabidopsis*, SI is controlled by a single genomic region "the *S* locus," which contains two tightly linked genes that encode the pollen *S*-locus cysteine-rich (SCR) and stigma *S*-locus receptor kinase (SRK) recognition proteins, whose ligand-receptor molecular docking leads to self-pollen rejection (*1*–*4*). The pollen recognition phenotype is controlled by the diploid paternal parent's genotype, but even though most plants are heterozygous at this locus (*5*), the pollen recognition phenotype is typically determined by one of the two alleles only, according to the alleles' relative positions in a hierarchy or network of dominance-recessivity interactions between *S* alleles (*6*). Selection is expected to favor genetic elements ("dominance modifiers"), which establish dominance-recessivity interaction rather than codominance, because individuals with a codominant genotype can produce pollen rejected by more potential mates than would occur in a dominant-recessive system (*7*, *8*). On the basis of modeling (*8*), the large nonrecombining region composing the *S* locus (*9*–*11*) is a strong candidate region for hosting such genetic elements.

Until recently, the dominance modifiers assumed in models (*7*, *8*) remained hypothetical. A particular small RNA (sRNA) has been identified (*12*) within the *S* locus of dominant alleles in Brassica (called *Smi*). This sRNA acts as a trans-modifier of the gene controlling pollen specificity via de novo methylation of the promoter of recessive alleles, which leads to transcriptional silencing of recessive alleles by dominant alleles (*13*, *14*). However, the mechanism in the more complex dominance-recessivity networks in species that have many levels in the dominance hierarchy (*15*, *16*) is unknown. Indeed, balancing selection typically leads to the maintenance of a large number of *S* alleles in self-incompatible

[1]Laboratoire Génétique et Evolution des Populations Végétales, CNRS UMR 8198, Université Lille 1, F-59655 Villeneuve d'Ascq cedex, France. [2]Reproduction et Développement des Plantes, Institut Fédératif de Recherche 128, Centre National de la Recherche Scientifique, Institut National de la Recherche Agronomique, Université Claude Bernard Lyon I, Ecole Normale Supérieure de Lyon, F-69364 Lyon, Cedex 07, France. [3]Department of Biology, Swiss Federal Institute of Technology Zurich, CH-8093 Zurich, Switzerland. [4]UDSL Université Lille 2 Droit et Santé, and Plate-forme de génomique fonctionnelle et structurale IFR-114, F-59000 Lille, France. [5]Centre National des Ressources Génomiques Végétales, INRA UPR 1258, Castanet-Tolosan, France.
*These authors contributed equally to this work. †Deceased.
‡Corresponding author. E-mail: vincent.castric@univ-lille1.fr

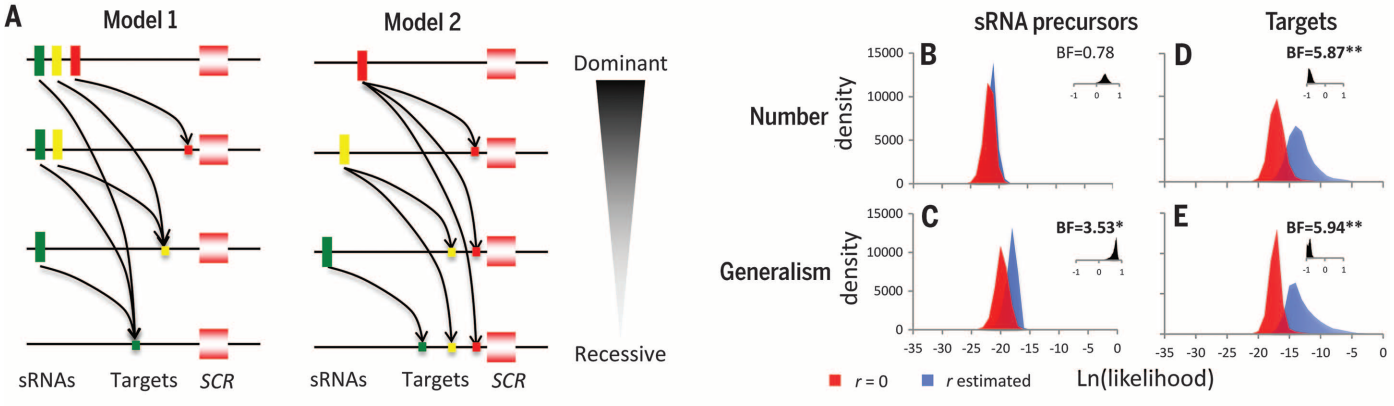

Fig. 1. Models for the control of dominance-recessivity by sRNA-target interactions in a multiallelic system. (**A**) Two models were tested to explain how a simple mechanistic model (*12*) can be generalized to a multiallelic system. Under model 1, dominant *S* alleles carry a larger set of sRNA precursor genes, whereas, under model 2, the same linear hierarchy is achieved by a larger set of sRNA targets carried by recessive *S* alleles. Under model 1, sRNA targets of recessive alleles are also more "generalist" than those of dominant alleles, whereas, under model 2, it is the sRNA precursors of the dominant alleles that are more generalist. (**B** to **E**) Likelihood distributions of Bayesian models if one assumes no correlation or allows for some level of correlated evolution between: (B) dominance and the number of sRNAs precursors expressed; (C) dominance and sRNA generalism, defined as the average number of targets used per sRNA precursor; (D) dominance and the number of target sites; and (E) dominance and target sites generalism, defined as the average number of distinct sRNA precursors using each target. The Bayes factor (BF) comparing both models is given on each panel as asterisks, as well as the distribution of correlation coefficients. *BF > 2: evidence for the dependent model, **BF > 5: strong evidence, and ***BF > 10: very strong evidence (*38*).

species, and the >50 *S* alleles observed in outcrossing *Arabidopsis* species (*17*) are predicted to form up to 1225 distinct heterozygous genotypes. In Brassica, class II alleles similarly show a linear dominance hierarchy that cannot be explained by the action of *Smi* alone (*12*, *18*). Under the mechanistic model involving sRNAs and their targets within the *SCR* gene, two hypotheses could explain an allelic series of *n* distinct *S* alleles in a linear dominance hierarchy. First, the most-dominant allele might produce *n* – 1 distinct sRNAs, each specifically targeting a given more-recessive *S* allele, whereas the next-most-dominant allele might produce sRNAs targeting all *S* alleles more recessive than itself, and so on (with the bottom recessive producing no sRNAs but having targets for all more-dominant alleles). This model predicts that the top dominant allele produces the largest number of sRNAs and that the bottom recessive allele carries the fewest but is targeted by the largest number of sequences; we refer to this as model 1 (Fig. 1A). Alternatively, the most dominant allele might produce a single sRNA, as in Brassica (*12*), and all subsequent more-recessive *S* alleles might carry a specific target that interacts with the most-dominant allele in a manner that results in nonexpression (Fig. 1A); the next allele in the hierarchy (that is recessive to the top dominant, but dominant to other classes) might produce a different sRNA, whose target sequence is present in all alleles recessive to itself, and so on. This model (model 2 in Fig. 1A) predicts that only a single sRNA is produced in all but the most-recessive allele, where the most-recessive allele carries the largest number of target sequences (each targeted by a different dominant allele).

Results

Phenotypic characterization of the dominance network

To determine the mechanisms of *S*-allele dominance in the self-incompatible plant *Arabidopsis halleri*, we first phenotypically characterized the dominance network between six *S* alleles, by crossing each of the 15 heterozygous genotypic combinations to both of its respective "tester" lines (i.e., lines that express a single *S* allele) (*19*). Overall, combining these results with those from previous studies (*16*), we determined all possible pairwise relations and observed dominance in 14 cases (93.3%) and codominance for a single case (Fig. 2A). The resulting network is fully transitive and takes the form of a simple linear hierarchy with two alleles at the top of the hierarchy (Ah13 and Ah20) (Fig. 2B).

S locus–specific sRNA precursor genes

We then examined the highly differentiated nonrecombining region within the *S* locus (*9*) (Fig. 3A) and deep-sequenced sRNA populations of floral buds (*19*) from 11 individuals carrying the six *S* alleles in various heterozygous combinations. Applying a set of criteria for annotating plant micro-RNA (miRNA) genes (*19*, *20*), we identified a total of 17 sRNA precursor sequences among the six tested alleles (Fig. 3B and fig. S2), with an average of about 2.8 sRNA precursors per allele (Fig. 3B). Given the large number of *S* alleles segregating in natural populations of *A. halleri* (*17*), this is fewer than expected if dominant alleles targeted each individual recessive allele by a distinct sRNA gene (as predicted from model 1).

The 17 expressed motifs (Fig. 3B) can be classified into eight distinct families on the basis of sequence divergence (fig. S3). Three of these families (*mir1887*, *mir4239*, and *mir867*) have clear homology to miRNA genes annotated in the *A. thaliana* genome and are present in the miRBase database (*21*), although it is unclear whether they should be considered bona fide miRNA genes, especially because it has been suggested that *Smi* might achieve silencing through a different—largely uncharacterized—sRNA pathway (*22*). In *A. thaliana*, these miRNA genes were all in the region flanked by *At4g21350* and *At4g21380*, which contains the relics of the degenerate *S* locus (*23*). Although their function has not been assessed so far, our results suggest that these motifs may have served as modifiers of *S*-allele dominance, consistent with the fact that the *A. thaliana S* locus has only recently undergone degeneration (*24*). The five other families we identified have no homology to any sequence in miRBase.

Identification and functional validation of sRNA-target interactions

The model proposed in *Brassica* was from observations of specific targeting of the promoter region of recessive *SCR* alleles involving sequences in recessive alleles showing similarity with the 24–nucleotide (nt) sRNA produced by dominant ones (*12*). We therefore searched for similarities between sRNA sequences produced by the 17 sRNA precursors identified above and sequences within 1 kilobase (kb) on either side of the six *SCR* alleles, where the majority of regulatory elements and, thus, potential target sites of the sRNAs are most likely to be found (*25*–*27*). In total, with stringent alignment criteria (*28*) (alignment threshold = 18), we identified potentially strong signals for 21 pairwise sRNA-*SCR* interactions (Fig. 3B and fig. S4), greater than expected on the basis of randomized sequences with nucleotide composition identical to that of real *SCR* sequences (fig. S5). Thus, *SCR* sequences appear to be highly enriched in sRNA target sites.

We focused on one specific sRNA-target interaction to validate in planta the regulatory effect of the sRNA gene on its target. The SI system can be transferred in *A. thaliana*, a self-fertile species, by transformation with the *SRK-SCR* genes from self-incompatible Brassicaceae (*29*), and the SI response is particularly robust and stable on stage 13 stigmas from the C24 ecotype (*30*, *31*). We thus transformed C24 *A. thaliana* plants with either *AhSRK01* or *AhSCR01*, i.e., the female and male determinants, respectively, of the most recessive *S* allele, Ah01 (*19*). Pollen from the hemizygous *AhSCR01*-transformed line was rejected on stage 13 stigmas from the *AhSRK01*-transformed line but was functional on wild-type (WT) stigmas, which demonstrated a reconstructed SI response (Fig. 4A and table S1) (*19*). We then tested the effect of the *mirS3* sRNA precursor gene produced by Ah20 (*Ah20mirS3*), which we

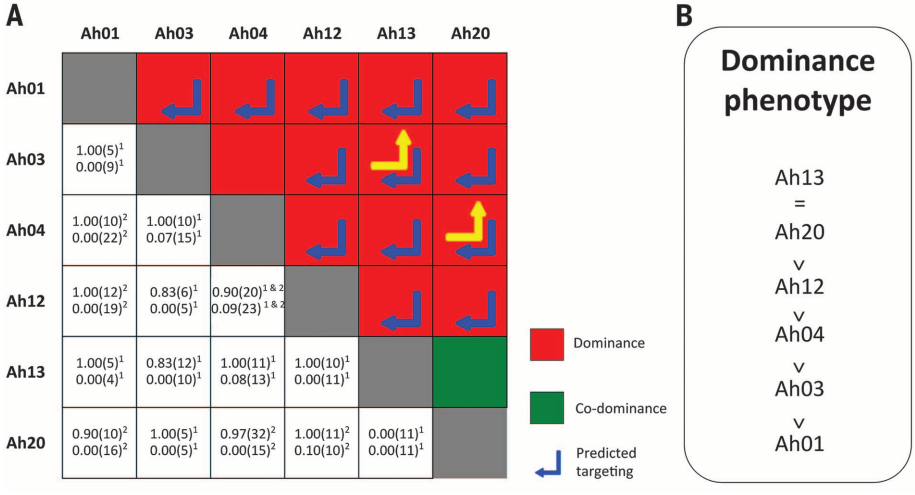

Fig. 2. Phenotypic network of dominance-recessivity interactions between alleles. (**A**) Dominance network obtained by controlled crosses and comparison with the molecular model. Below the diagonal, the proportion of compatible crosses on female tester lines of the column allele is given first for each heterozygote combination, followed by the proportion of compatible crosses on female tester lines of the row allele. Numbers in parentheses indicate the number of replicate crosses to determine the proportion in each type of crosses. Superscripts indicate the source of the data: 1, present study; 2, (*16*). Above the diagonal, pairwise dominance interactions, as inferred from the crosses, are represented in red and codominance in green. Blue arrows indicate that the column allele is producing a sRNA that is predicted to target the row allele. Yellow arrows indicate that the row allele is producing a sRNA that is predicted to target the column allele (Smith and Waterman stringency threshold = 18). (**B**) Controlled crosses (detailed in Fig. 2) can be represented as a linear dominance hierarchy among the six *S* alleles.

predicted to be the genetic element causing dominance of Ah20 over Ah01 (Figs. 2A and 3B). We generated *Ah20mirS3 A. thaliana* transgenic lines, which we crossed with the *AhSCR01* line to obtain hybrid plants containing the two transgenes in hemizygous state (i.e., as biologically relevant for *S* alleles) (table S1) (*19*). Pollen from these hybrid plants could germinate on *AhSRK01* stigmas, which showed that the presence of *Ah20mirS3* was sufficient to abolish the SI response conferred by *AhSCR01* alone (Mood's median test *P* value = 2.2×10^{-4} and 3.2×10^{-5} on two replicate *Ah20mirS3* insertion lines) (Fig. 4A). Finally, we produced a mutated *AhSCR01* line (*AhSCR01**) in which we introduced a set of four point mutations specifically in the *Ah20mirS3* predicted target (located in the intron of *AhSCR01*) (Figs. 3B and 4B), which we crossed with lines containing *Ah20mirS3*. As expected, pollen from the *AhSCR01* Ah20mirS3* hybrid plants was insensitive to the effect of *Ah20mirS3* and was rejected on *AhSRK01* stigmas. Hence, our data demonstrate that our predicted target site for *AhSCR01* was necessary for the regulatory effect of *Ah20mirS3* (Fig. 4B). Note that sRNA target sites within introns of genes have already been observed and validated experimentally, in a different context (*32*). Overall, our validation procedure provides direct experimental support to identify sRNA genes and their target sites, although a complete experiment involving all 21 predicted sRNA-target interactions would arguably be required to fully validate the proposed regulatory mechanism between the six *S* alleles.

Power and accuracy of the molecular model

We evaluated power and accuracy of our model of dominance-recessivity interactions by comparing molecular predictions with the phenotypic observations from controlled crosses. With two exceptions, most (93.1%) of the predictions connect a sRNA produced by a dominant allele to a target present in a more-recessive allele above the proportion expected by chance alone (about 63 to 79%, obtained by 100,000 random permutations) (fig. S6), which suggests that our molecular prediction of target sites is reliable, with a low false-positive rate. Overall, 13 of the 14 dominance-recessivity relations observed in our tests (93%) were predicted by at least one sRNA targeting prediction (Fig. 2A), which suggests that sRNAs can explain the majority of the interactions we observe at the phenotypic level. Thus, a simple molecular model explaining the control of dominance through factors closely linked to the *S* locus can predict observed dominance phenotypes.

A single interaction (Ah04>Ah03) remains unexplained by this simple mechanism. We thus enlarged our search to sRNA reads in the *S* locus that are not derived from hairpins. Because of the high transposable element (TE) content of the *S* locus (*9*), such small interfering RNAs (siRNAs) are particularly abundant in the region. Collectively, siRNAs seem to target dominant alleles about as frequently as recessive alleles (fig. S6) and are very close to random expectations, which suggests that, even though some of them may indeed regulate dominance, most of them are probably derived from the TE control machinery with no specific role in controlling dominance-recessivity interactions. In the case of the unexplained Ah04>Ah03 interaction, none of the siRNAs produced by Ah04 is predicted to target *AhSCR03* (fig. S7). It is possible that another sRNA, whose low abundance may remain undetected, is controlling dominance of Ah04 over Ah03.

Dominance and recessivity—More sRNAs or more targets?

Given the diversity of both sRNA precursors and their targets, we asked whether the position of *S* alleles along the dominance hierarchy is explained by models 1 or 2 (Fig. 1A), i.e., by number or by "generalism" (the ability of their resulting

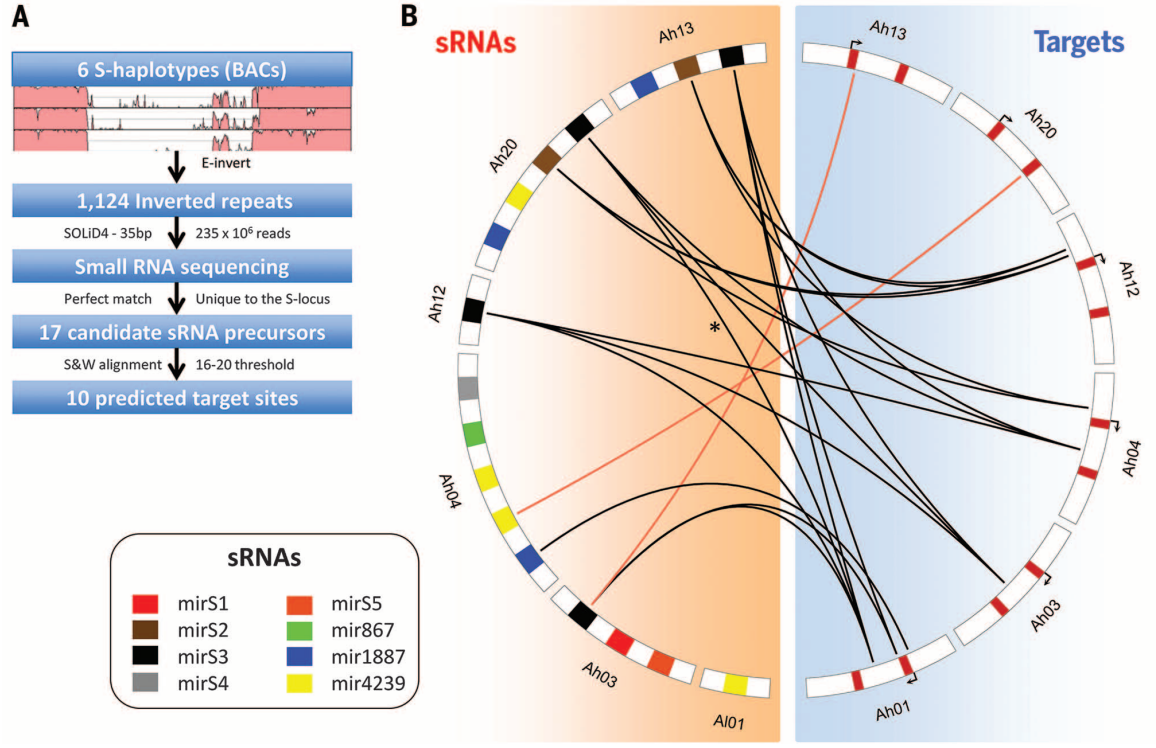

Fig. 3. Regulatory network determined from sRNAs and their predicted targets in *A. halleri*. (**A**) Flowchart of the annotation procedure of sRNA precursors. (**B**) Repertoire of sRNAs precursors and their predicted targets. sRNA precursors carried by each *S* allele are represented on the left. Precursor families are color-coded, and the correspondence between colors and precursor families is given in the box on the bottom left. sRNA targets on the *SCR* gene (±1 kb) are represented on the right. *S* alleles are displayed according to their position along the dominance hierarchy represented on Fig. 2B (dominant alleles on top, recessive alleles at the bottom). Red boxes on the target side correspond to the two exons on *SCR*, with arrows giving the direction of transcription. For clarity, length variation of the *SCR* intron is not represented. A line joins a precursor with a target whenever the precursor produces a sRNA that is predicted to use that target (based on an alignment threshold of 18). Black and red lines represent targeting relations that are and are not consistent with the phenotypic network, respectively. The star symbol indicates the sRNA-target interaction that we functionally validate in Fig. 4 (*Ah20mirS3* on *AhSCR01*).

sRNAs to target a broader spectrum of *S* alleles) of the sRNA precursors and the targets they carry. Taking the phylogeny of the *S* alleles into account, we compared with Bayes factors (BFs) if the sRNA precursors or their inferred targets evolve in a correlated manner with dominance or if they are independent. We detected an asymmetry between the functional evolution of sRNAs and that of their targets. Overall, we confirmed that sRNA precursors in dominant *S* alleles are predicted to target more *S* alleles than those of recessive alleles [BF = 21.7***, correlation coefficient (r) = 0.99] (fig. S8) [for the explanation of asterisk indications, see the legend to (Fig. 1)]. However, dominant *S* alleles do not do this by increased total numbers of sRNA precursors [BF = 0.78 (not significant), r = 0.33] (Fig. 1B) but rather by greater sRNA precursor generalism (BF = 3.53*, r = 0.64) (Fig. 1C). In contrast, the observed increased degree to which recessive alleles are targeted by sRNAs (BF = 21.7***, r = −0.99) (fig. S8) appears to have involved both increased total numbers of targets (BF = 5.87**, r = −0.81) (Fig. 1D) and increased generality of each target (BF = 5.94**, r = −0.84) (Fig. 1E). Overall, our results support model 2, with the addition that several sRNA precursors cooperate to provide the full targeting spectrum of dominant alleles. However, targets carried by recessive alleles have wider spectra than those of more-dominant alleles, a feature of model 1.

Evolution by gain and loss

To infer the evolutionary changes in the regulatory network in a broader phylogenetic context, we inspected the repertoire of sRNA precursors and their targets on a set of 14 additional *S* alleles from bacterial artificial chromosome (BAC) sequences for the *S* locus [(*9*, *10*, *33*) and this study]. sRNA precursor genes were inferred from sequence similarity with the 17 sRNA genes examined, plus the *Smi* sRNA precursor of *Brassica* (*12*). Overall, the 20 *S* alleles yielded 86 putative sRNA genes with sequence similarity to either *Smi* or one of the eight sRNA families (Fig. 5 and fig. S3). From the six *S* alleles for which small RNA–sequencing (sRNA-seq) data were available, 23 sequence motifs were detected from this homology search. Hence, six motifs were present in addition to the 17 sRNA precursors in Fig. 3B but not supported by sRNA reads, which suggested that some of these elements may be expressed at levels too low to detect by sRNA-seq. Notably, although significant hits of *Smi* motifs were identified in seven different *A. halleri S* alleles, none of them was expressed at a detectable level. In some *S* alleles, several of these "silent" motifs have as many predicted targets as expressed motifs from the same family (fig. S9), but on average, these motifs tend to have fewer predicted targets than those that are expressed (fig. S9). This finding suggests that these sRNA genes may have undergone functional degeneration with decreased targeting ability, which may suggest a turnover of active sRNA genes on the *S* alleles.

The presence or absence of the 86 putative sRNA genes was consistent with the phylogeny of the different alleles from the *SRK* gene, which suggested that interallelic recombination at the *S* locus in SI lineages is infrequent (*9*–*11*). Accordingly, ancestral states reconstruction inferred the most likely scenario of gains and losses of the different precursors in a Bayesian framework (Fig. 5 and fig. S10) (*19*). This reconstruction indicates that some sRNA precursor families (*mirS2*, *mirS3*, and *mir4239*) are ancient and can be traced back to the most recent common ancestor of all extant *S* alleles. In contrast, several precursor families seem to have evolved more recently, during the diversification of this species' *S* alleles (*mirS1*, *mir867*, *mirS4*, and *mirS5*) and are found only in the two lineages of more-recessive alleles [classes II and III, according to (*15*)] (Fig. 5). For the two remaining families (*mirSmi* and *mir1887*) ancestral reconstruction indicates multiple independent origins on different alleles, although horizontal transfer by occasional recombination between *S* alleles may also potentially explain this pattern. Repertoires of precursors on the different *S* alleles were also modified in the course of evolution by repeated deletions, and we infer at least eight independent deletion events. Finally, some precursor families seem to have been expanded by duplication, as several *S* haplotypes have multiple paralogs of a given sRNA precursor family (up to four *mir4239* precursors on allele Al13) (Fig. 5).

Reconstruction of ancestral states is more challenging for the sRNA targets, because of their more-variable phylogenetic distribution. From our analyses, we observed that evolution of the newly arisen *mir867* precursor—from the common ancestor of Ah04, Ah10, and Al16—and acquisition of the *mirS4* precursor by Ah04 are both associated with the acquisition of their cognate targets on the respective branch from the same ancestral node, which indicated that allelic diversification was closely followed by the emergence of sRNA-target interactions. At least one target is also inferred to be ancient (that of *mirS3* in the intron of *SCR*), which suggested that there may be functional constraint over evolutionary times. No putative target could be identified for *mirS1* and *mirS5*, which may control dominance over currently unidentified alleles known to exist in the species (*17*, *34*).

Evolutionary conservation of the sRNA genes

To evaluate functional constraints of the sRNA motifs, we compared sequence divergence between functional orthologs of the *S*-locus region

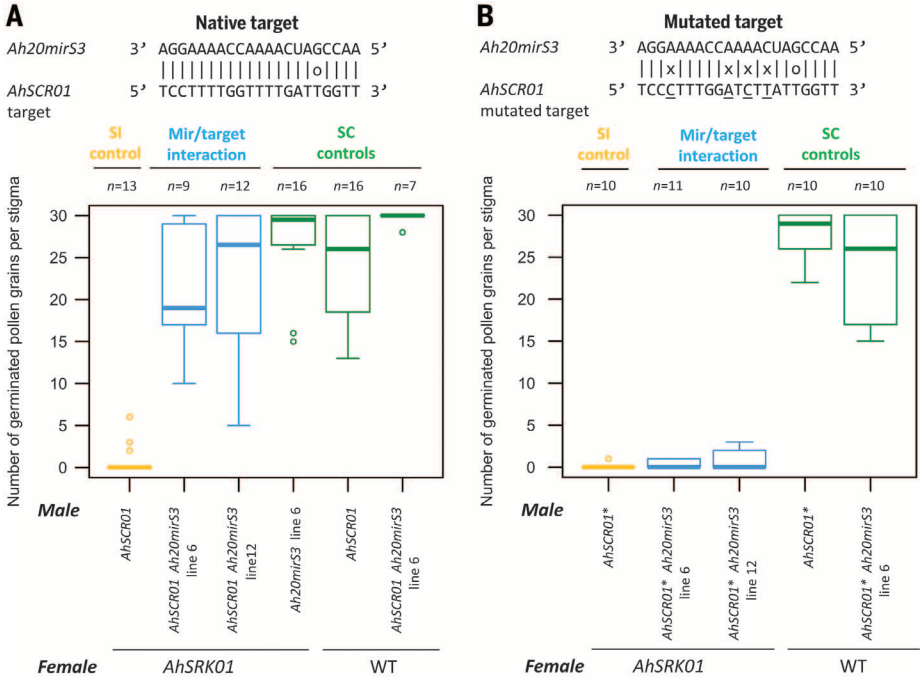

Fig. 4. *In planta* functional validation that Ah20 controls phenotypic expression of *SCR01* through specific targeting by *mirS3*. (**A**) *Ah20mirS3* is sufficient to abolish the SI response of *AhSCR01*. (**B**) The mutated target makes *AhSCR01** insensitive to the effect of *Ah20mirS3*. Pollen compatibility was estimated by the number of germinated pollen grains per stigma. Incompatible crosses (SI) are colored in yellow-orange, compatible controls (SC) in green, and tests of the mir-target interactions in blue (see table S1). Mir-target interactions were tested on hybrids produced from two *Ah20mirS3*-independent insertion lines, named lines 6 and 12. Thick bars represent the median, boxes the interquartile range, whiskers extend out 1.5 times the interquartile range, and individual points are outliers. The number of replicates (n) is indicated above each cross. (A) (Top) The most abundant targeting sRNA produced by the *Ah20mirS3* precursor is aligned with the *SCR01* predicted target; in (B), it is aligned with the mutated target. Mismatches are represented by "x," and G:U wobbles by "o." Mutated bases are underlined.

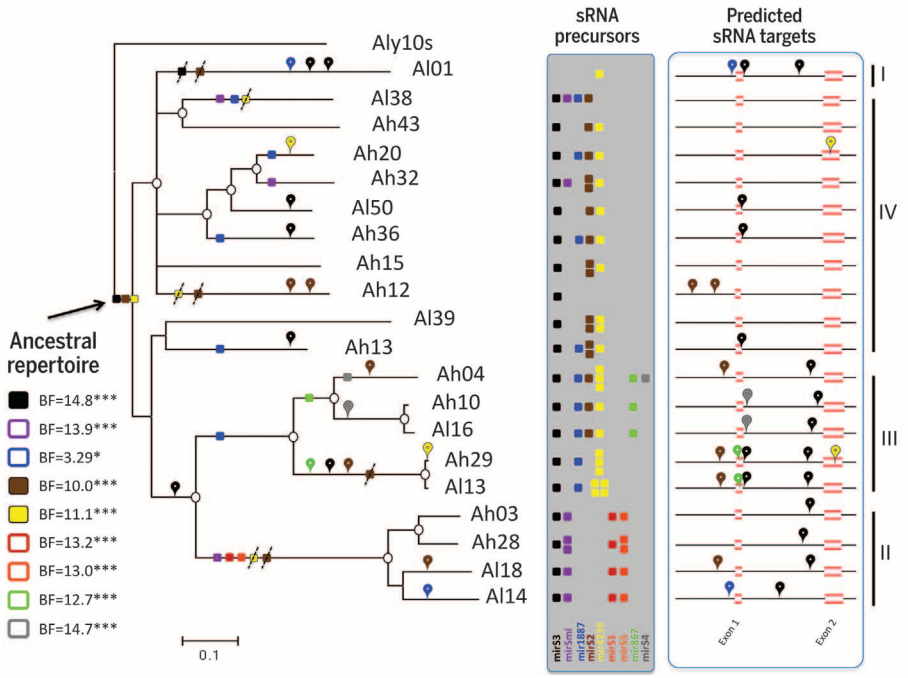

Fig. 5. Repertoire of sRNA genes and their targets along the phylogeny of *S* alleles. The Bayesian phylogeny is based on full *A. halleri* and *A. lyrata SRK* amino acid sequences. Node support was assessed by posterior probabilities (PP), and nodes with PP > 0.95 are represented by white circles. Phylogenetic classes are reported (I, II, III, and IV) (*15*). The scenario of gain and loss for sRNA precursors and their targets is represented on the branch where each event is inferred. Solid and open squares indicate precursors that are inferred to have been present and absent from the ancestral repertoire, respectively. For each precursor, asterisks for BFs indicate the level of confidence on the presence or absence from the ancestral repertoire. *BF > 2: some evidence, **BF > 5: strong evidence, and ***BF > 10: very strong evidence (*38*).

in *A. halleri*, *A. lyrata*, and *A. thaliana* (*17*). As a whole, this nonrecombining region includes large amounts of noncoding and repetitive sequences and displays extremely high levels of sequence divergence (*9*) (fig. S11). However, the two protein-coding genes in the region, *SCR* and *SRK*, as well as the set of sRNA precursors, form islands of sequence conservation, even in the comparison with *A. thaliana*, over at least 10 million years, which suggests that substantial functional constraints exist on these motifs, at least comparable to that acting upon the protein-coding genes controlling SI specificity.

Conclusions

The molecular mechanisms of genetic dominance (and its flip side, recessivity), integral to Mendel's discoveries, have been strongly debated. For deleterious mutations, this debate was largely resolved by the understanding that physiological properties of metabolic pathways rather than dominance modifiers (i.e., genetic elements controlling the dominance of genes) explain many, if not all, dominance-recessivity interactions in genomes (*35*). For balanced polymorphisms, however, dominance modifiers could evolve under natural selection in theoretical models (*36*, *37*), and our analysis now provides a molecular basis for most of the control of dominance levels for SI. Although regulatory networks have typically been viewed as arising between genes in a genome, we present a surprisingly complex example of a regulatory network among alleles at a single genetic locus. Moreover, as predicted theoretically, the sRNA genes that we identified as involved in the control of dominance are found within the *S*-locus region.

An interesting question is how natural selection has shaped the genetic elements controlling this network. Although our empirical results support the theoretical predictions cited above, there is a major difference between the single dominance modifiers assumed by the models and the system of interacting sequences that produce the actual *SCR* dominance relations in *A. halleri*; the system of sRNAs and their targets entails a coevolutionary process between the two interacting partners, which is not found in previous models (*7*, *8*). Such a coevolutionary process could potentially correspond either to an evolutionary arms race (with dominant *S* alleles accumulating sRNA genes, whereas recessive ones escape silencing by mutations in their targets) or to a mutualistic system. One can argue that the latter is more likely because the models show that natural selection on this type of SI system mostly acts against codominance and that dominance and recessivity are both equally advantageous (*7*, *8*). When such data will be extended to more alleles, it will be interesting to compare the results with further theoretical expectations based on evolutionary arms race or mutualistic interactions models.

REFERENCES AND NOTES

1. C. R. Schopfer, M. E. Nasrallah, J. B. Nasrallah, *Science* **286**, 1697–1700 (1999).
2. S. Takayama *et al.*, *Proc. Natl. Acad. Sci. U.S.A.* **97**, 1920–1925 (2000).
3. J. C. Stein, B. Howlett, D. C. Boyes, M. E. Nasrallah, J. B. Nasrallah, *Proc. Natl. Acad. Sci. U.S.A.* **88**, 8816–8820 (1991).
4. T. Takasaki *et al.*, *Nature* **403**, 913–916 (2000).
5. D. De Nettancourt, *Incompatibility and Incongruity in Wild and Cultivated Plants* (Springer-Verlag, Berlin, 2001).
6. A. J. Bateman, *Heredity* **9**, 53–68 (1955).
7. V. Llaurens, S. Billiard, V. Castric, X. Vekemans, *Evolution* **63**, 2427–2437 (2009).
8. D. J. Schoen, J. W. Busch, *Evolution* **63**, 2099–2113 (2009).
9. P. M. Goubet *et al.*, *PLOS Genet.* **8**, e1002495 (2012).
10. Y. L. Guo, X. Zhao, C. Lanz, D. Weigel, *Plant Physiol.* **157**, 937–946 (2011).
11. G. Suzuki *et al.*, *Genetics* **153**, 391–400 (1999).
12. Y. Tarutani *et al.*, *Nature* **466**, 983–986 (2010).
13. H. Shiba *et al.*, *Plant Cell* **14**, 491–504 (2002).
14. H. Shiba *et al.*, *Nat. Genet.* **38**, 297–299 (2006).
15. N. L. Prigoda, A. Nassuth, B. K. Mable, *Mol. Biol. Evol.* **22**, 1609–1620 (2005).
16. V. Llaurens *et al.*, *Evolution* **62**, 2545–2557 (2008).
17. V. Castric, J. Bechsgaard, M. H. Schierup, X. Vekemans, *PLOS Genet.* **4**, e1000168 (2008).
18. H. Shiba, S. Takayama, *Dev. Growth Differ.* **54**, 120–128 (2012).
19. Materials and methods are available as supplementary materials on *Science* Online.
20. B. C. Meyers *et al.*, *Plant Cell* **20**, 3186–3190 (2008).
21. A. Kozomara, S. Griffiths-Jones, *Nucleic Acids Res.* **39** (Database), D152–D157 (2011).
22. E. J. Finnegan, D. Liang, M. B. Wang, *Trends Plant Sci.* **16**, 238–241 (2011).
23. X. Vekemans, C. Poux, P. M. Goubet, V. Castric, *J. Evol. Biol.* **27**, 1372–1385 (2014).
24. J. S. Bechsgaard, V. Castric, D. Charlesworth, X. Vekemans, M. H. Schierup, *Mol. Biol. Evol.* **23**, 1741–1750 (2006).
25. T. R. O'Connor, C. Dyreson, J. J. Wyrick, *Bioinformatics* **21**, 4411–4413 (2005).
26. G. Zeller *et al.*, *Genome Res.* **18**, 918–929 (2008).
27. W. Zhang, T. Zhang, Y. Wu, J. Jiang, *Plant Cell* **24**, 2719–2731 (2012).
28. T. F. Smith, M. S. Waterman, *J. Mol. Biol.* **147**, 195–197 (1981).
29. M. E. Nasrallah, P. Liu, J. B. Nasrallah, *Science* **297**, 247–249 (2002).
30. M. E. Nasrallah, P. Liu, S. Sherman-Broyles, N. A. Boggs, J. B. Nasrallah, *Proc. Natl. Acad. Sci. U.S.A.* **101**, 16070–16074 (2004).
31. N. A. Boggs, J. B. Nasrallah, M. E. Nasrallah, *PLOS Genet.* **5**, e1000426 (2009).
32. Y. Meng, C. Shao, X. Ma, H. Wang, *Rice* **6**, 8 (2013).
33. T. T. Hu *et al.*, *Nat. Genet.* **43**, 476–481 (2011).
34. B. K. Mable, M. H. Schierup, D. Charlesworth, *Heredity* **90**, 422–431 (2003).
35. H. C. Bagheri, *J. Exp. Zoolog. B Mol. Dev. Evol.* **306B**, 329–359 (2006).
36. S. P. Otto, D. Bourguet, *Am. Nat.* **153**, 561–574 (1999).
37. S. Billiard, V. Castric, *Trends Genet.* **27**, 441–445 (2011).
38. M. Pagel, A. Meade, *Am. Nat.* **167**, 808–825 (2006).

ACKNOWLEDGMENTS

We thank D. Charlesworth, T. Tsuchimatsu, M. Boccara, D. J. Schoen, and M. Mirouze for advice and comments on the manuscript and J. Kitt, A. C. Holl, E. Schmitt, B. Huss, G. Neutelings, A. Achard, G. Laroche, and D. Achour for technical assistance. We acknowledge financial support from Agence Nationale de la Recherche Jeunes Chercheurs BRASSIDOM (ANR 11 JSV7-008-01), *Bonus Qualité Recherche* Université Lille 1 and Région Nord Pas de Calais (program "projets

émergents" MICRO2). R.M. was supported by an apprentice grant from CNRS. R.M. and E.D. contributed equally to this work. E.D. contributed to the crossing design and the phenotypic analysis. R.M., E.D., M.S., P.M.G., and S.G. contributed to the bioinformatics analysis. E.D., I.F.-L., E.G., and T.G. performed the functional validation experiment. C.P. performed the phylogenetic analysis. M.F. performed the sRNA-seq experiments. E.P., W.M., and H.B. constructed the BAC libraries and performed the screening and BAC sequencing. V.C., S.B., X.V., I.F.-L., and T.G. designed the experiments. All authors discussed the results. E.D., R.M., I.F.-L., X.V., S.B., and V.C. wrote the paper. V.C. and S.B. coordinated the project. *S*-locus sequences have been deposited on the European Molecular Biology Organization public database, sRNA sequences on the GEO public database (see table S2 for accession numbers), and data matrices and phylogenetic trees on the TreeBASE database (http://purl.org/phylo/treebase/phylows/study/TB2:S16394). BAC clones produced in this project will be distributed through http://cnrgv.toulouse.inra.fr/Library/Arabidopsis upon signature of a material transfer agreement for in-house academic research.

SUPPLEMENTARY MATERIALS

www.sciencemag.org/content/346/6214/1200/suppl/DC1
Materials and Methods
Figs. S1 to S12
Tables S1 and S2
References (*39*–*57*)

31 July 2014; accepted 17 October 2014
10.1126/science.1259442

REPORTS

VALLEYTRONICS

Ultrafast generation of pseudo-magnetic field for valley excitons in WSe_2 monolayers

Jonghwan Kim,[1]* Xiaoping Hong,[1]* Chenhao Jin,[1] Su-Fei Shi,[1,2] Chih-Yuan S. Chang,[3] Ming-Hui Chiu,[4] Lain-Jong Li,[3,4] Feng Wang[1,2,5]†

The valley pseudospin is a degree of freedom that emerges in atomically thin two-dimensional transition metal dichalcogenides (MX_2). The capability to manipulate it, in analogy to the control of spin in spintronics, can open up exciting opportunities. Here, we demonstrate that an ultrafast and ultrahigh valley pseudo-magnetic field can be generated by using circularly polarized femtosecond pulses to selectively control the valley degree of freedom in monolayer MX_2. Using ultrafast pump-probe spectroscopy, we observed a pure and valley-selective optical Stark effect in WSe_2 monolayers from the nonresonant pump, resulting in an energy splitting of more than 10 milli–electron volts between the K and K′ valley exciton transitions. Our study opens up the possibility to coherently manipulate the valley polarization for quantum information applications.

Atomically thin layers of transition metal dichalcogenides (MX_2) have emerged as an exciting two-dimensional semiconductor platform for nanoelectronics and optoelectronics (*1*, *2*). In particular, a pair of degenerate bands are present at the K and K′ valleys in the momentum space of hexagonal MX_2 monolayers, giving rise to a valley degree of freedom that is analogous to electron spin (*3*). Recent polarization-resolved photoluminescence (PL) studies show that the valley pseudospin in MX_2 can couple directly to the helicity of excitation photons (*4*–*7*) and that the pseudospin polarization between two valleys exhibits coherent behavior (*7*). It raises the intriguing prospect of valleytronics, which exploits the valley degree of freedom to carry information (*1*, *3*–*9*).

Just as spin manipulation is essential in spintronics, the capability to control the valley pseudospin is essential for valleytronics based on MX_2 materials. In spintronics, the electron spin can be manipulated through any external perturbation that breaks the energy degeneracy of two orthogonal spin polarizations. This can be achieved either through an external magnetic field (*10*, *11*) or through a pseudo-magnetic field generated by other stimuli. For example, circularly polarized light can produce a pseudo-magnetic field that can be used to manipulate electron spins in semiconductor quantum wells and quantum dots (*12*, *13*) through the optical Stark effect. (The optical Stark effect, a well-established phenomenon in atomic physics and quantum optics, describes the energy shift in a two-level system induced by a nonresonant laser field.) It is highly desirable to realize similar control of valley excitons in MX_2 by using light-induced pseudo-magnetic field for valleytronics.

[1]Department of Physics, University of California at Berkeley, Berkeley, CA 94720, USA. [2]Material Science Division, Lawrence Berkeley National Laboratory, Berkeley, CA 94720, USA. [3]Institute of Atomic and Molecular Sciences, Academia Sinica, Taipei 10617, Taiwan. [4]Physical Sciences and Engineering, King Abdullah University of Science and Technology, Thuwal, Saudi Arabia. [5]Kavli Energy NanoSciences Institute, University of California Berkeley and Lawrence Berkeley National Laboratory, Berkeley, CA 94720, USA.
*These authors contributed equally to this work, **†Corresponding author. E-mail: fengwang76@berkeley.edu**

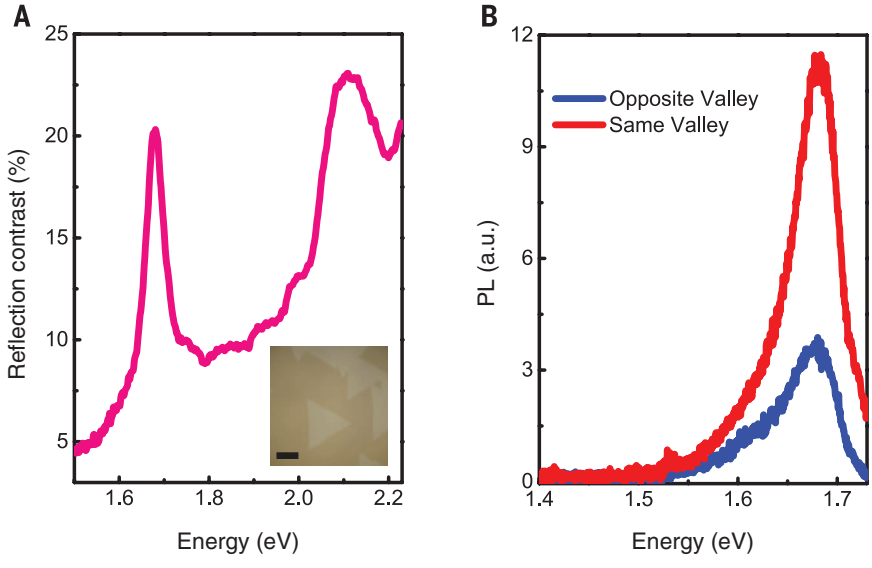

Fig. 1. Valley exciton transitions in monolayer WSe_2. (**A**) The optical reflection spectrum of a WSe_2 monolayer on a sapphire substrate at 77 K. It shows strong A- and B-exciton resonances at 1.68 and 2.1 eV, respectively. (Inset) Optical microscopy image of the sample. Scale bar, 25 μm. (**B**) Polarization-resolved PL spectra of a WSe_2 monolayer at 77K. For a 1.8-eV excitation laser with left circular polarization, the PL spectra show a prominent emission peak at the A-exciton resonance (1.68 eV), and the PL intensity with left circular polarization (red curve) is about four times stronger than that with right circular polarization (blue curve). It demonstrates that valley-polarized A-exciton population can be created by circularly polarized resonant excitation and it can be detected with polarization-resolved PL spectroscopy.

Dominance hierarchy arising from the evolution of a complex small RNA regulatory network

Eléonore Durand *et al.*

Science **346**, 1200 (2014);
DOI: 10.1126/science.1259442

Science (print ISSN 0036-8075; online ISSN 1095-9203) is published weekly, except the last week in December, by the American Association for the Advancement of Science, 1200 New York Avenue NW, Washington, DC 20005.